

Geometric scaling of elastic pp cross section at the LHC

Michał Przaszałowicz¹

*Institute of Theoretical Physics, Faculty of Physics, Astronomy and Applied Computer Science,
Jagiellonian University, S. Łojasiewicza 11, 30-348 Kraków, Poland.*

Abstract

We show that geometric scaling conjectured and observed at the ISR more than 50 years ago, still holds at the LHC. We discuss regularities of the dip-bump structures of the differential elastic cross sections, emphasizing the fact that the ratio of bump to dip positions is constant from the ISR to the LHC. Applying crossing and analyticity we identify imaginary and real parts of the scattering amplitude and compute the ρ parameter and the ratio of bump to dip values of the differential pp cross sections. We also discuss the energy dependence of the total elastic cross section and the violation of geometrical scaling outside the dip-bump region at the LHC.

Keywords: elastic pp scattering, geometrical scaling

1. Introduction

In this paper we argue that geometric scaling conjectured and observed at the ISR more than 50 years ago [1, 2], still holds at the LHC. This is not so obvious, since recent attempts to find a scaling law for elastic pp cross sections at the LHC energies have pointed to a different scaling [3, 4], possibly associated with high energy saturation [5]. For other studies on scaling properties of elastic cross sections see [6, 7].

There exist three sets of total and two of differential pp high energy data. The ISR data [8, 9] collected at CERN in 1970's cover energies $20 \text{ GeV} \lesssim W = \sqrt{s} \lesssim 60 \text{ GeV}$, recent LHC data by the TOTEM [10, 11, 12, 13] and ATLAS [14, 15, 16] Collaborations at $3 \text{ TeV} \lesssim W = \sqrt{s} \lesssim 13 \text{ TeV}$ and the cosmic rays total cross section data, which, however, have rather large errors (see Fig. 2).

Starting from the ISR energies total pp cross sections rise with energy, but the increase is faster at the LHC than at the lower energies. To show this in Ref. [4] a power law fit was performed in the restricted energy ranges, separately for the ISR data [9] and for the LHC data [17]. The results are shown in Table 1. One can see that at the ISR all pp cross sections (total, elastic and inelastic) increase with energy with a universal power of $\simeq 0.11$, which led to the formulation of geometric scaling (GS) in the 1970's [1, 2]. This is no longer true at the LHC, casting doubt on the possibility that GS still holds at the LHC [3, 4].

	elastic	inelastic	total	ρ
ISR	$W^{0.1142 \pm 0.0034}$	$W^{0.1099 \pm 0.0012}$	$W^{0.1098 \pm 0.0012}$	0.02 – 0.095
LHC	$W^{0.2279 \pm 0.0228}$	$W^{0.1465 \pm 0.0133}$	$W^{0.1729 \pm 0.0163}$	0.15 – 0.10

Table 1: Energy dependence of the integrated pp cross sections for the energies $W = \sqrt{s}$ at the ISR [9] and at the LHC [17], and the ρ parameter [9, 18]. Table from Ref. [4].

GS for the integrated cross sections can be best visualized in the impact parameter space. To see this, let's consider the textbook formulas for the total and elastic cross sections in the normalization, where the

¹michal.praszalowicz@uj.edu.pl

scattering amplitude is dimensionless

$$\begin{aligned}\sigma_{\text{tot}}(s) &= 2 \int d^2\mathbf{b} \operatorname{Im} T_{\text{el}}(s, b), \\ \sigma_{\text{el}}(s) &= \int d^2\mathbf{b} |T_{\text{el}}(s, b)|^2.\end{aligned}\tag{1}$$

Inelastic cross-section is given as $\sigma_{\text{inel}}(s) = \sigma_{\text{tot}}(s) - \sigma_{\text{el}}(s)$.

GS in impact parameter space means that $\operatorname{Im} T_{\text{el}}(s, b) = \operatorname{Im} T_{\text{el}}(b/R(s))$, where $R(s)$ is a so called interaction radius to be determined from the data [1]. It follows that the amplitude, which is formally a function of two independent variables b and s , depends in fact only on one dimensionless scaled variable $B(s) = b/R(s)$. Changing variables in the first equation (1) $b \rightarrow B = b/R(s)$ one obtains

$$\sigma_{\text{tot}}(s) = 2R^2(s) \int d^2\mathbf{B} \operatorname{Im} T_{\text{el}}(B).\tag{2}$$

If the real part of the elastic scattering amplitude can be neglected, as suggested by the smallness of the parameter $\rho = \operatorname{Re} T_{\text{el}}(s, t = 0) / \operatorname{Im} T_{\text{el}}(s, t = 0)$ in momentum space, see Table 1, we get that also $\sigma_{\text{el}}(s) \sim R^2(s)$ and as a consequence also $\sigma_{\text{inel}}(s) \sim R^2(s)$. As mentioned above GS of integrated cross sections is clearly seen at the ISR, but not at the LHC.

2. Elastic differential cross section and the dip-bump structure

Let us now recall main features of pp differential elastic cross section $d\sigma_{\text{el}}/dt$. One observes a rapid decrease for small $|t|$, then a minimum at t_{dip} , followed by a broad maximum at t_{bump} . This dip-bump structure emerges, as we will see later, from the Fourier transform of the impact parameter amplitude [19] and is related to the zeros and extrema of J_0 Bessel function. A universal and striking property was reported in Ref. [4], namely that the ratio of bump to dip *positions* is constant over the large energy span from the ISR to the LHC

$$\mathcal{T}_{\text{bd}}(s) = |t_{\text{bump}}|/|t_{\text{dip}}| = 1.355 \pm 0.011.\tag{3}$$

On the contrary, the ratio of the cross section *values*

$$\mathcal{R}_{\text{bd}}(s) = \frac{d\sigma_{\text{el}}/d|t|_{\text{bump}}}{d\sigma_{\text{el}}/d|t|_{\text{dip}}},\tag{4}$$

which saturates at the LHC energies at a value of approximately 1.8, is rather strongly energy dependent at the ISR (see e.g. Fig. 2 in Ref. [20] and Fig 4).

Property (3) implies that dip and bump positions should be identical at all energies if $d\sigma_{\text{el}}/dt$ is plotted in terms of a scaling variable $\tau = f(s)|t|$. In order to find $f(s)$ at the LHC Ref. [4] performed a power law fit to the dips $|t_{\text{dip}}| = \text{const} \times (W/(1 \text{ TeV}))^{-\beta}$ with the result $\beta = 0.1686 \pm 0.0037$ and $\text{const} = 0.732 \pm 0.003 \text{ GeV}^2$. Therefore $f(s) \sim W^\beta$. Bumps are reproduced due to the property (3). Note that, within experimental accuracy, β is equal to exponent of the total cross section (see Table 1). Hence from Eq. (2) we can take $f(s) = R^2(s) \sim \sigma_{\text{tot}}(s)$.

At the ISR the situation is very similar. The authors of Ref. [2] used $R^2(s) \sim \sigma_{\text{inel}}(s)$, however, since the energy dependence of σ_{inel} and σ_{tot} is the same, they could have used $f(s) = R^2(s) \sim \sigma_{\text{tot}}(s)$ as well, which they did in Ref. [21].

In order to further discuss GS it is more convenient to work in the momentum representation

$$T_{\text{el}}(s, b) = \int \frac{d^2\mathbf{q}}{(2\pi)^2} e^{i\mathbf{b}\mathbf{q}} T_{\text{el}}(s, t).\tag{5}$$

Here $b = |\mathbf{b}|$, $t = -\mathbf{q}^2$. Then, from Eq. (1)

$$s\sigma_{\text{tot}}(s) = 2 \operatorname{Im} \tilde{T}_{\text{el}}(s, 0).\tag{6}$$

Following Refs. [1, 2] we prefer work in a normalization where the elastic amplitude is dimensionless $\tilde{T}_{\text{el}}(s, t) = sT_{\text{el}}(s, t)$. In this normalization the total elastic cross-section reads

$$\sigma_{\text{el}}(s) = \frac{1}{4\pi s^2} \int dt \left| \tilde{T}_{\text{el}}(s, t) \right|^2. \quad (7)$$

Now, we would like to parametrize $\tilde{T}_{\text{el}}(s, t)$ in a way which explicitly obeys GS and reproduces the energy dependence of the total cross section (6), neglecting for the moment the real part. In momentum representation GS means that $\tilde{T}_{\text{el}}(s, t) \rightarrow \tilde{T}_{\text{el}}(s, \tau)$,² where $\tau = |t| R^2(s)$. Then, to recover the energy dependence $\sigma_{\text{tot}}(s) \sim R^2(s)$ in Eq. (6), we assume that (we will be more precise later)

$$\tilde{T}_{\text{el}}(s, \tau) = isR^2(s)\Phi(\tau). \quad (8)$$

Here $\Phi(\tau)$ is a dimensionless real function of the scaling variable τ .

Substituting (8) to Eq. (7) we get

$$\sigma_{\text{el}}(s) = \frac{R^2(s)}{4\pi} \int d\tau \Phi^2(\tau). \quad (9)$$

We see that the energy dependence of $\sigma_{\text{el}}(s)$ is indeed, as at the ISR, the same as $\sigma_{\text{tot}}(s)$. We will discuss later why this relation may be broken at the LHC.

To proceed further, let us observe that function $\Phi(\tau)$ must have at least one zero [19, 21]. Indeed, taking an inverse Fourier transform of (5) we obtain

$$\Phi(\tau) = 2\pi \int dB B J_0(B\sqrt{\tau}) \text{Im} T_{\text{el}}(B). \quad (10)$$

Since $\text{Im} T_{\text{el}}(B)$ is typically a smooth localized function (for example in the black disc toy model $\text{Im} T_{\text{el}}(B) \sim \Theta(1 - B)$), function $\Phi(\tau)$ has zeros corresponding to the zeros of the Bessel function J_0 . Notably, the first zero corresponds to the dip of the amplitude square [19, 21]. At this point we cannot neglect the real part. Further, the minimum of the amplitude after the first zero corresponds to the bump in the cross section.

It is instructive to illustrate this in the black disc approximation, where

$$\Phi(\tau) = 2\pi \frac{J_1(\sqrt{\tau})}{\sqrt{\tau}}, \quad (11)$$

which is plotted in the left panel of Fig. 1. In the right panel we plot Φ^2 , which is responsible for the imaginary part contribution to the cross section. Therefore we have

$$\Phi(\tau_{\text{dip}}) = 0, \quad \frac{d}{d\tau} \Phi(\tau)|_{\text{bump}} = 0. \quad (12)$$

To include the real part of T_{el} we have to impose crossing symmetry [19] on (8). In the Regge limit (all masses equal zero, $s \gg -t$) the crossing relation takes the following form

$$\tilde{T}_{\text{el}}(u, t) \simeq \tilde{T}_{\text{el}}(-s, t) = \tilde{T}_{\text{el}}^*(s, t). \quad (13)$$

Therefore, following [19, 21] we assume

$$\tilde{T}_{\text{el}}(s, \tau) = isR^2(-is)\Phi\left(|t|R^2(-is)\right), \quad (14)$$

which satisfies (13). We will now identify real and imaginary parts of the amplitude observing that

$$-is = e^{y-i\pi/2}. \quad (15)$$

²Dependence of $\tilde{T}_{\text{el}}(s, \tau)$ on s is only in the normalization factor.

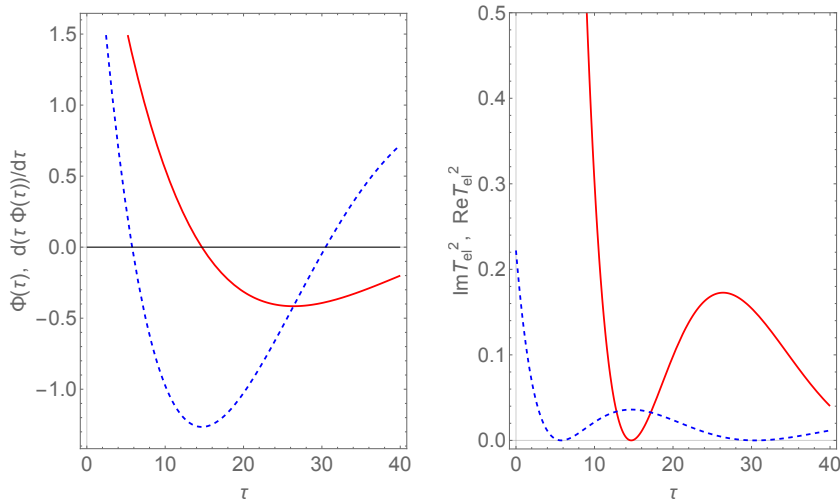


Figure 1: Left panel: function $\Phi(\tau)$ from Eq. (11) – solid red line, and $d(\tau\Phi(\tau))/d\tau$ – dashed blue. Right panel: Contributions of imaginary (solid red) and real (dashed blue) parts of the scattering amplitude to the elastic cross section. For the real part the ρ parameter is 0.15.

Expressing R^2 in terms of rapidity $y = \ln s$ rather than s , and expanding, we get [19]

$$R^2(-is) \rightarrow R^2\left(y - i\frac{\pi}{2}\right) \simeq R^2(y) - i\frac{\pi}{2} \frac{dR^2(y)}{dy}. \quad (16)$$

Expanding further we arrive at

$$\Phi\left(|t| R^2(-is)\right) \simeq \Phi(\tau) - i\frac{\pi}{2} \frac{d\Phi(\tau)}{d\tau} \frac{dR^2(y)}{dy} |t|. \quad (17)$$

Keeping only linear terms from expansions (16) and (17) we get [19, 21]

$$\begin{aligned} \text{Im } \tilde{T}_{\text{el}}(s, \tau) &= sR^2(y)\Phi(\tau), \\ \text{Re } \tilde{T}_{\text{el}}(s, \tau) &= s\frac{\pi}{2} \frac{dR^2(y)}{dy} \frac{d}{d\tau} (\tau\Phi(\tau)). \end{aligned} \quad (18)$$

In Fig. 1 we plot both $\Phi(\tau)$ and $d(\tau\Phi(\tau))/d\tau$ for the hard disc toy model (11), and – in the right panel – the corresponding contributions to the cross section. We see that the cross section is dominated by the imaginary part squared, except for the dip, where the real part dominates (for illustration purposes we have assumed $\rho = 0.15$).

3. Comparison with the data

Formulas (18) result in an absolute prediction for the ρ parameter

$$\rho = \frac{\text{Re } \tilde{T}_{\text{el}}(s, \tau = 0)}{\text{Im } \tilde{T}_{\text{el}}(s, \tau = 0)} = \frac{\pi}{2} \frac{1}{R^2(y)} \frac{dR^2(y)}{dy}. \quad (19)$$

Relation (19) has been derived, at least parametrically, from the dispersion relations long time ago (see e.g. Ref. [22]). However, it is instructive to compare it with the current data. For illustration purposes we use two analytic parametrizations of the total pp cross section. The first one is the COMPETE parametrization [23] quoted in PDG 2010 [24]

$$\sigma_{\text{tot}}^{\text{PDG}}(s) = Z + C \ln^2\left(\frac{s}{s_0}\right) + Y_1 \left(\frac{s}{s_1}\right)^{-\eta_1} - Y_2 \left(\frac{s}{s_1}\right)^{-\eta_2}, \quad (20)$$

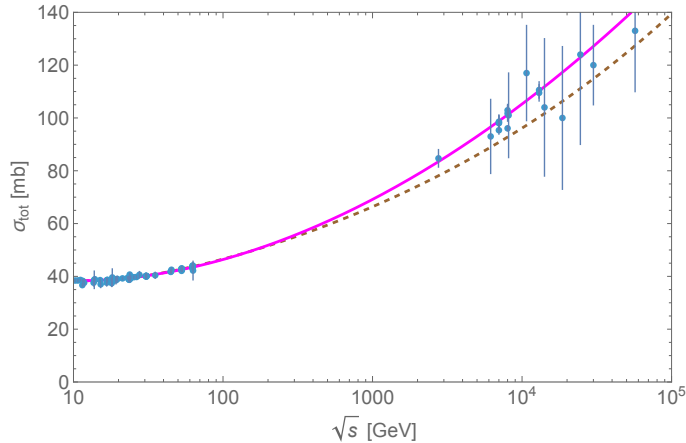


Figure 2: Total pp cross-section in mb as a function of \sqrt{s} in GeV. Points at small $\sqrt{s} < 100$ GeV are from the ISR, points above 1 TeV are from the LHC (small error bars) and from cosmic rays. Solid magenta line corresponds to the PDG parametrization (20) and brown dashed line to (21).

where $Z = 35.45$ mb, $C = 0.308$ mb, $Y_1 = 42.53$ mb, $Y_2 = 33.34$ mb, $s_0 = 28.94$ GeV², $s_1 = 1$ GeV² and $\eta_1 = 0.458$, $\eta_2 = 0.545$. The second one is from Ref. [25] by Donnachie and Landshoff

$$\sigma_{\text{tot}}^{\text{DL}}(s) = A \left(\frac{s}{s_1} \right)^\alpha + B \left(\frac{s}{s_1} \right)^\beta, \quad (21)$$

where $A = 21.70$ mb, $B = 56.08$ mb, $\alpha = 0.0808$, $\beta = -0.4525$ and $s_1 = 1$ GeV². They are plotted in Fig. 2 together with data points (see the web page of PDG 2022 [26]). One can see that the PDG parametrization (20) covers the whole energy range from the ISR to the LHC (including the $p\bar{p}$ data not shown on the plot), whereas the older parametrization by Donnachie and Landshoff (21) devised to describe low energy data undershoots the LHC points.

In Fig. 3 we plot the parameter ρ computed according to Eq. (19) together with the data [26]. We can see that the PDG parametrization (20) describes the ρ parameter rather well. Note that both normalization and the energy dependence are reproduced without any adjustable parameter. The last two points in Fig. 3 correspond to two different estimates by TOTEM [12]. The fact that they are lower than our predictions (and, in fact, lower than in many other more precise models and parametrizations) has led to the conjecture that this deviation is a sign of the odderon [7, 20, 22, 27] (see however [28, 29]). If so, our analysis should be extended to include the C parity odd amplitude, which is beyond the scope of the present study.

Now, from Eq. (12) we can compute ratio $\mathcal{R}_{\text{bd}}(s)$ (4). Indeed, we have

$$\begin{aligned} \Phi(\tau_{\text{dip}}) = 0 &\rightarrow \text{Im } \tilde{T}_{\text{el}}(s, \tau_{\text{dip}}) = 0, \\ \text{Re } \tilde{T}_{\text{el}}(s, \tau_{\text{dip}}) &= s \frac{\pi}{2} \frac{dR^2(y)}{dy} \frac{d}{d\tau} \Phi(\tau_{\text{dip}}), \end{aligned} \quad (22)$$

and

$$\begin{aligned} \frac{d}{d\tau} \Phi(\tau_{\text{bump}}) = 0 &\rightarrow \text{Im } \tilde{T}_{\text{el}}(s, \tau_{\text{dip}}) = s R_1^2(y) \Phi(\tau_{\text{bump}}), \\ \text{Re } \tilde{T}_{\text{el}}(s, \tau_{\text{dip}}) &= s \frac{\pi}{2} \frac{dR^2(y)}{dy} \Phi(\tau_{\text{bump}}). \end{aligned} \quad (23)$$

Therefore

$$\left. \frac{d\sigma}{dt} \right|_{\text{dip}} = \frac{R^4(y)}{4\pi} \rho^2(y) \left(\tau_{\text{dip}} \frac{d}{d\tau} \Phi(\tau_{\text{dip}}) \right)^2 \quad (24)$$

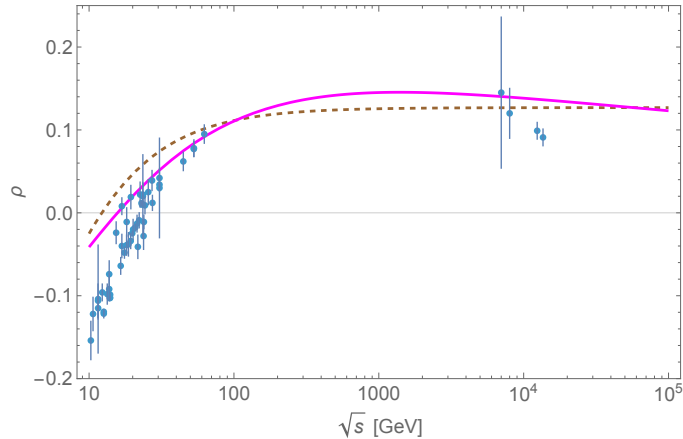


Figure 3: Parameter ρ (19) as a function of \sqrt{s} in GeV. Points at small $\sqrt{s} < 100$ GeV are from the ISR, points above 1 TeV are from the LHC. Solid magenta line corresponds to the PDG parametrization (20) and brown dashed line to (21).

and

$$\left. \frac{d\sigma}{dt} \right|_{\text{bump}} = \frac{R^4(y)}{4\pi} (1 + \rho^2(y)) \Phi^2(\tau_{\text{bump}}). \quad (25)$$

Hence, we have a one parameter prediction for the ratio

$$\mathcal{R}_{\text{bd}}(s) = \frac{d\sigma/dt(t_{\text{bump}})}{d\sigma/dt(t_{\text{dip}})} = c_0 \frac{1 + \rho^2(y)}{\rho^2(y)}, \quad (26)$$

where constant c_0 is given in terms of function Φ

$$c_0 = \frac{\Phi^2(\tau_{\text{bump}})}{(\tau_{\text{dip}} \frac{d}{d\tau} \Phi(\tau_{\text{dip}}))^2}. \quad (27)$$

In Fig. 4 we plot ratio (26) for two parametrizations (20) and (21) with $c_0 = 0.012 \div 0.013$. One can see that the ratio data are well reproduced by both parametrizations.

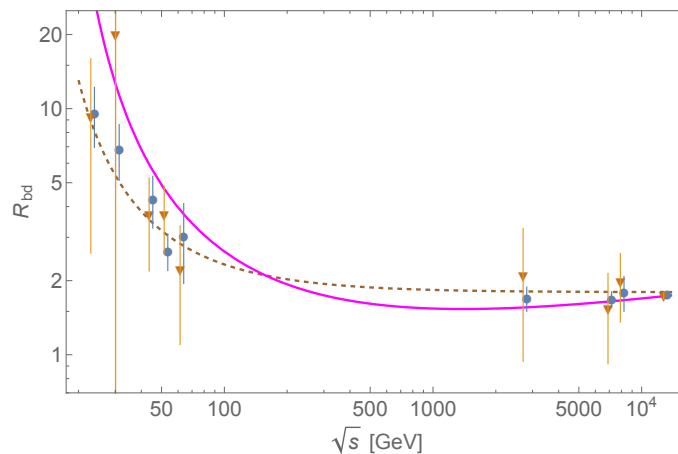


Figure 4: Ratio \mathcal{R}_{bd} as a function of \sqrt{s} in GeV. Data: brown triangles from Ref. [4], blue circles from Ref. [20]. Theoretical curves (26) as in Figs. 2 and 3.

And finally we can compute the energy dependence of the total elastic cross section

$$\begin{aligned}\sigma_{\text{el}}(s) &= \frac{1}{4\pi R^2(y)} \left[R^4(y) \int d\tau \Phi^2(\tau) + \left(\frac{\pi}{2} \frac{dR^2(y)}{dy} \right)^2 \int d\tau \left(\frac{d}{d\tau} (\tau \Phi(\tau)) \right)^2 \right] \\ &= \frac{R^2(y)}{4\pi} (1 + c_1 \rho^2(y)) \times \int d\tau \Phi^2(\tau),\end{aligned}\quad (28)$$

where

$$c_1 = \frac{\int d\tau \left(\frac{d}{d\tau} (\tau \Phi(\tau)) \right)^2}{\int d\tau \Phi^2(\tau)}.\quad (29)$$

We see from Eq. (29) that the energy dependence of the total elastic pp cross section is modified with respect to the total cross section by a factor

$$\frac{\sigma_{\text{el}}(s)}{\sigma_{\text{tot}}(s)} \sim (1 + c_1 \rho^2(s)).\quad (30)$$

At the ISR the ρ parameter is very small and, despite the fact that it rapidly rises with energy, its influence on σ_{el} is negligible.³ At the LHC the ρ parameter is slightly larger but it is almost constant (see Fig. 3) and therefore does not modify the energy dependence of σ_{el} as well. This result is of course in conflict with the data. However, note that formula (29) assumes that GS is valid *everywhere* in t . This is certainly not true outside the dip-bump region, although at the ISR GS surprisingly holds down to a very small t [4]. Therefore, the inability of GS to describe the energy dependence of the total elastic cross section at the LHC should be attributed to the GS violation outside the dip-bump region, most importantly at small t .

4. Summary and discussion

To summarize: we have shown that properties of the dip-bump structures of the differential elastic cross sections can be interpreted assuming geometric scaling both at the ISR and at the LHC. The scaling variable is $\tau \sim \sigma_{\text{tot}}(s)|t|$. Assuming GS and crossing, and applying expansion (16) and (17) we have been able to identify imaginary and real parts of the scattering amplitude and derive formulas for the parameter ρ and the ratio \mathcal{R}_{bd} , which reproduce the data, despite the fact that the analysis presented here, which extends the approach of Refs. [1, 2, 19, 21] to the LHC, is only of qualitative character. Therefore, one should not expect too high accuracy when comparing with the data. The energy dependence of the total elastic pp cross section is, however, not reproduced. We have attributed this to the GS violation outside the dip-bump region, at small values of t , which dominate the total elastic cross section. Indeed, it is well known, that the phenomenological formula

$$\frac{\sigma_{\text{el}}(s)}{\sigma_{\text{tot}}(s)} \sim \frac{\sigma_{\text{tot}}(s)}{B(s)} (1 + \rho^2(s)),\quad (31)$$

where $B(s)$ is a slope of the diffractive peak, works very well to an accuracy of a few percent (see e.g. [30, 31]). In deriving the formula (31) one basically neglects the dip-bump structure taking into account only the diffraction peak, which gives the dominant contribution to the total elastic cross section, in a form which does not exhibit GS [30].

At this point it is interesting to compare our results with the so called H scaling proposed in Ref. [7], where function $H(x)$ defined as

$$H(x) = \frac{1}{B(s)\sigma_{\text{el}}(s)} \frac{d\sigma_{\text{el}}}{dt}(s, t)\quad (32)$$

³To be more quantitative we need to compute c_1 .

should depend on the scaling variable $x = B(s)|t|$ alone. At small t we can neglect the real part of the scattering amplitude where, if GS holds, the cross section reads

$$\frac{d\sigma_{\text{el}}}{dt}(s, t) = \frac{\sigma_{\text{tot}}^2(s)}{4\pi} \Phi^2(\tau), \quad (33)$$

and

$$H(x) = \frac{1}{4\pi} \frac{\sigma_{\text{tot}}^2(s)}{B(s)\sigma_{\text{el}}(s)} \Phi^2(\tau). \quad (34)$$

However, asymptotically $\sigma_{\text{tot}}(s)/\sigma_{\text{el}}(s) \rightarrow \text{const.}$ and $\sigma_{\text{tot}}(s)/B(s) \rightarrow \text{const.}$ [30], hence $x \rightarrow \tau$ and the H scaling and GS coincide. The difference in sub-asymptotic energies is of course important for phenomenology. To account for a difference between $B(s)$ and $\sigma_{\text{tot}}(s)$ one could use the property known as the stationary point, which provides a relation between these two quantities, which is valid from the ISR to the LHC [32].

The above discussion shows that in order to improve phenomenology of GS one needs to include GS violations at small t . It would be interesting to extend the present study to the $p\bar{p}$ case, and to include the odderon amplitude. One may also try to find corrections to the expansions (16) and (17).

Acknowledgments

The author acknowledges CERN TH Department for hospitality while this research was being carried out, and would like to thank T. Csörgő, Ch. Royon and A. Staśto for discussions and remarks.

References

- [1] J. Dias De Deus, “Geometric Scaling, Multiplicity Distributions and Cross-Sections,” Nucl. Phys. B **59**, 231-236 (1973) doi:10.1016/0550-3213(73)90485-9
- [2] A. J. Buras and J. Dias de Deus, “Scaling law for the elastic differential cross-section in p p scattering from geometric scaling,” Nucl. Phys. B **71**, 481-492 (1974) doi:10.1016/0550-3213(74)90197-7
- [3] C. Baldenegro, C. Royon and A. M. Staśto, “Scaling properties of elastic proton-proton scattering at LHC energies,” Phys. Lett. B **830**, 137141 (2022) doi:10.1016/j.physletb.2022.137141 [arXiv:2204.08328 [hep-ph]].
- [4] C. Baldenegro, M. Praszalowicz, C. Royon and A. M. Staśto, “Scaling laws of elastic proton-proton scattering differential cross sections,” Phys. Lett. B **856**, 138960 (2024) doi:10.1016/j.physletb.2024.138960 [arXiv:2406.01737 [hep-ph]].
- [5] R. Peschanski and B. G. Giraud, “A QCD interpretation of the scaling observed in the LHC proton-proton elastic cross-sections at moderate transfer momentum,” [arXiv:2409.20153 [hep-ph]].
- [6] I. M. Dremin and V. A. Nechitailo, “Testing scaling laws for the elastic scattering of protons,” Phys. Lett. B **720**, 177-180 (2013) doi:10.1016/j.physletb.2013.02.012 [arXiv:1212.3313 [hep-ph]].
- [7] T. Csörgő, T. Novak, R. Pasechnik, A. Ster and I. Szanyi, “Evidence of Odderon-exchange from scaling properties of elastic scattering at TeV energies,” Eur. Phys. J. C **81**, no.2, 180 (2021) doi:10.1140/epjc/s10052-021-08867-6 [arXiv:1912.11968 [hep-ph]].
- [8] E. Nagy, R. S. Orr, W. Schmidt-Parzefall, K. Winter, A. Brandt, F. W. Busser, G. Flugge, F. Niebergall, P. E. Schumacher and H. Eichinger, *et al.* “Measurements of Elastic Proton Proton Scattering at Large Momentum Transfer at the CERN Intersecting Storage Rings,” Nucl. Phys. B **150**, 221-267 (1979) doi:10.1016/0550-3213(79)90301-8
- [9] U. Amaldi and K. R. Schubert, “Impact Parameter Interpretation of Proton Proton Scattering from a Critical Review of All ISR Data,” Nucl. Phys. B **166**, 301-320 (1980) doi:10.1016/0550-3213(80)90229-1
- [10] G. Antchev *et al.* [TOTEM], “Proton-proton elastic scattering at the LHC energy of $\sqrt{s} = 7$ -TeV,” EPL **95**, no.4, 41001 (2011) doi:10.1209/0295-5075/95/41001 [arXiv:1110.1385 [hep-ex]].
- [11] G. Antchev *et al.* [TOTEM], “Evidence for non-exponential elastic proton proton differential cross-section at low $-t$ — and $\sqrt{s}=8$ TeV by TOTEM,” Nucl. Phys. B **899**, 527-546 (2015) doi:10.1016/j.nuclphysb.2015.08.010 [arXiv:1503.08111 [hep-ex]].
- [12] G. Antchev *et al.* [TOTEM], “First determination of the ρ parameter at $\sqrt{s} = 13$ TeV: probing the existence of a colourless C-odd three-gluon compound state,” Eur. Phys. J. C **79**, no.9, 785 (2019) doi:10.1140/epjc/s10052-019-7223-4 [arXiv:1812.04732 [hep-ex]].
- [13] G. Antchev *et al.* [TOTEM], “Elastic differential cross-section $d\sigma/dt$ at $\sqrt{s} = 2.76$ TeV and implications on the existence of a colourless C-odd three-gluon compound state,” Eur. Phys. J. C **80**, no.2, 91 (2020) doi:10.1140/epjc/s10052-020-7654-y [arXiv:1812.08610 [hep-ex]].
- [14] G. Aad *et al.* [ATLAS], “Measurement of the total cross section from elastic scattering in pp collisions at $\sqrt{s} = 7$ TeV with the ATLAS detector,” Nucl. Phys. B **889**, 486-548 (2014) doi:10.1016/j.nuclphysb.2014.10.019 [arXiv:1408.5778 [hep-ex]].
- [15] M. Aaboud *et al.* [ATLAS], “Measurement of the total cross section from elastic scattering in pp collisions at $\sqrt{s} = 8$ TeV with the ATLAS detector,” Phys. Lett. B **761**, 158-178 (2016) doi:10.1016/j.physletb.2016.08.020 [arXiv:1607.06605 [hep-ex]].

- [16] G. Aad *et al.* [ATLAS], “Measurement of the total cross section and ρ -parameter from elastic scattering in pp collisions at $\sqrt{s} = 13$ TeV with the ATLAS detector,” *Eur. Phys. J. C* **83**, no.5, 441 (2023) doi:10.1140/epjc/s10052-023-11436-8 [arXiv:2207.12246 [hep-ex]].
- [17] F. J. Nemes [TOTEM], “Elastic and Total Cross-section Measurements by Totem,” *PoS DIS2019*, 065 (2019) doi:10.1142/9789811233913.0041
- [18] G. Antchev *et al.* [TOTEM], “First measurement of elastic, inelastic and total cross-section at $\sqrt{s} = 13$ TeV by TOTEM and overview of cross-section data at LHC energies,” *Eur. Phys. J. C* **79**, no.2, 103 (2019) doi:10.1140/epjc/s10052-019-6567-0 [arXiv:1712.06153 [hep-ex]].
- [19] J. Dias de Deus, “On the Real Part of a Geometrical Pomeron,” *Nuovo Cim. A* **28**, 114 (1975) doi:10.1007/BF02730400
- [20] V. M. Abazov *et al.* [TOTEM and D0], “Odderon Exchange from Elastic Scattering Differences between pp and $p\bar{p}$ Data at 1.96 TeV and from pp Forward Scattering Measurements,” *Phys. Rev. Lett.* **127**, no.6, 062003 (2021) doi:10.1103/PhysRevLett.127.062003 [arXiv:2012.03981 [hep-ex]].
- [21] J. Dias de Deus and P. Kroll, “Dips, Zeros and Large $-t-$ Behavior of the Elastic Amplitude,” *Acta Phys. Polon. B* **9** (1978), 157 WU B 77-8.
- [22] M. G. Ryskin, “Current Status of the Odderon,” [arXiv:2408.01990 [hep-ph]].
- [23] J. R. Cudell, V. Ezhela, P. Gauron, K. Kang, Y. V. Kuyanov, S. Lugovsky, B. Nicolescu and N. Tkachenko, “Hadronic scattering amplitudes: Medium-energy constraints on asymptotic behavior,” *Phys. Rev. D* **65**, 074024 (2002) doi:10.1103/PhysRevD.65.074024 [arXiv:hep-ph/0107219 [hep-ph]].
- [24] K. Nakamura *et al.* (Particle Data Group), *J. Phys. G* **37**, 075021 (2010), sec. 41, p. 10.
- [25] A. Donnachie and P. V. Landshoff, “Total cross-sections”, *Phys. Lett. B* **296**, 227-232 (1992) doi:10.1016/0370-2693(92)90832-O [arXiv:hep-ph/9209205 [hep-ph]].
- [26] R.L. Workman *et al.* (Particle Data Group), *Prog. Theor. Exp. Phys.* **2022**, 083C01 (2022), <https://pdg.lbl.gov/2022/hadronic-xsections/hadron.html>
- [27] E. Martynov and B. Nicolescu, “Did TOTEM experiment discover the Odderon?,” *Phys. Lett. B* **778** (2018), 414-418 doi:10.1016/j.physletb.2018.01.054 [arXiv:1711.03288 [hep-ph]].
- [28] V. A. Khoze, A. D. Martin and M. G. Ryskin, *Phys. Rev. D* **97** (2018) no.3, 034019 doi:10.1103/PhysRevD.97.034019 [arXiv:1712.00325 [hep-ph]].
- [29] V. A. Khoze, A. D. Martin and M. G. Ryskin, *Phys. Lett. B* **784** (2018), 192-198 doi:10.1016/j.physletb.2018.07.054 [arXiv:1806.05970 [hep-ph]].
- [30] M. M. Block, “Hadronic forward scattering: Predictions for the Large Hadron Collider and cosmic rays,” *Phys. Rept.* **436** (2006), 71-215 doi:10.1016/j.physrep.2006.06.003 [arXiv:hep-ph/0606215 [hep-ph]].
- [31] W. Broniowski, L. Jenkovszky, E. Ruiz Arriola and I. Szanyi, “Hollowness in pp and $p\bar{p}$ scattering in a Regge model,” *Phys. Rev. D* **98** (2018) no.7, 074012 doi:10.1103/PhysRevD.98.074012 [arXiv:1806.04756 [hep-ph]].
- [32] A. P. Samokhin and V. A. Petrov, “The Stationary Points and Structure of High-Energy Scattering Amplitude,” *Nucl. Phys. A* **974** (2018), 45-55 doi:10.1016/j.nuclphysa.2018.03.009 [arXiv:1708.02879 [hep-ph]].